Journal of Magnetism and Magnetic Materials 380 (2015) 163–167

Contents lists available at ScienceDirect

Journal of Magnetism and Magnetic Materials

journal homepage: www.elsevier.com/locate/jmmm

How temperature determines formation of maghemite nanoparticles

Matthias Girod, Stefanie Vogel, Wojciech Szczerba, Andreas F. Thünemann *

BAM Federal Institute for Materials Research and Testing, Unter den Eichen 87, 12205 Berlin

ARTICLE INFO

Article history:
Received 27 June 2014
Received in revised form
15 September 2014
Accepted 29 September 2014
Available online 1 October 2014

Keywords:
Iron Oxide Nanoparticles
Micromixer
SAXS
XANES
Carboxydextran

ABSTRACT

We report on the formation of polymer-stabilized superparamagnetic single-core and multi-core maghemite nanoparticles. The particle formation was carried out by coprecipitation of Fe(II) and Fe(III) sulfate in a continuous aqueous process using a micromixer system. Aggregates containing 50 primary particles with sizes of 2 nm were formed at a reaction temperature of 30 °C. These particles aggregated further with time and were not stable. In contrast, stable single-core particles with a diameter of 7 nm were formed at 80 °C as revealed by small-angle X-ray scattering (SAXS) coupled in-line with the micromixer for particle characterization. X-ray diffraction and TEM confirmed the SAXS results. X-ray absorption near-edge structure spectroscopy (XANES) identified the iron oxide phase as maghemite.

1. Introduction

Magnetic colloids, also known as magnetic fluids or ferrofluids, consist of surface-coated magnetic nanoparticles dispersed in a liquid carrier. Magnetic fluids have a wide range of applications including heat and mass transfer applications such as liquid cooled loudspeakers and high power transformators [1,2], environmental applications like water cleaning [3] and biomedical applications. This last topic is probably one of the most appealing research areas. Applications on stem cell labeling [4], metastasis diagnostics [5], in vitro biodetection [6] and even in vivo cancer treatment [7] have been reported.

The crystal formation in solution is of key importance for generation of nanoparticles for these applications. Nucleation of small crystals from solution is classically described by the spontaneous formation of a nucleus that grows when it exceeds a critical size, which is determined by the surface energy to bulk energy ratio [8]. If several solid phases are possible, the formation of the thermodynamically stable phase can be preceded by metastable intermediates that stepwise transform to the final product. This is known as Ostwald's step rule, which states that phases more similar to the solution structure form more readily [9]. Further nucleation and growth often do not occur through the addition of atoms or molecules but may also involve aggregation and coalescence of small clusters. Such mechanisms have been termed as non-classical because they cannot be described within the classical nucleation and growth framework [10].

Here, we study the formation of iron oxide nanoparticles by coprecipitation of Fe(II) and Fe(III) sulfate at different temperatures in a micromixer. This is a continuous aqueous process which is monitored online by coupling with SAXS. To the best of our knowledge, using a micromixer and quick SAXS, is reported for the first time.

2. Materials and methods

2.1. Materials

Ammonium hydroxide, ferric sulfate hexahydrate ($Fe_2(SO_4)_3$ $6H_2O$) and ferrous sulfate tetrahydrate (($Fe(SO_4)4H_2O$) of analytical grade was purchased from Aldrich. Carboxydextran with a molar mass of 40×10^3 g mol^{-1} was purchased from Maito Sangyo, Japan.

2.2. Experimental setup

The experimental setup used for the synthesis of iron oxide nanoparticles is shown schematically in Fig. 1. It has two reservoirs: the first contains an aqueous solution of the iron salts and carboxydextran, the second contains ammonium hydroxide solution. Both reservoirs are connected via two HPLC pumps (Merck/Germany) with a reactor system composed of a micromixer and a microcapillary reactor. The micromixer is a caterpillar-type mixer (R600) made of polychlorotrifluoroethylene (PCTFE), purchased from the Institut für Mikrotechnik Mainz, Germany. The mixing principle of the micromixer was described in detail elsewhere [11].

* Corresponding author.
E-mail address: andreas.thuenemann@bam.de (A.F. Thünemann).

http://dx.doi.org/10.1016/j.jmmm.2014.09.057
0304-8853/

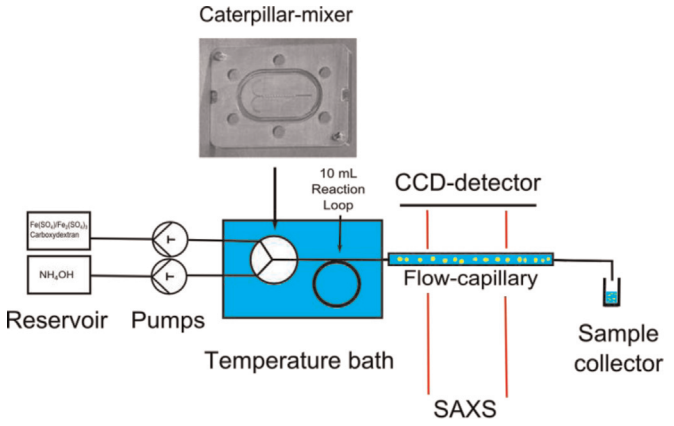

Fig. 1. Experimental setup for the continuous synthesis of polymer stabilized iron-oxide nanoparticles. The microreactor is directly connected to the SAXS device via PEEK tubing for particle characterization. The size of the microreactor is about 6.4 cm × 4.8 cm.

The microcapillary was made of stainless steel with a diameter of 750 µm and a total volume of 10 mL. The complete reaction system was placed in a temperature bath (Huber CC-318B, Germany) and interconnected with a quartz flow capillary (inner diameter 1 mm and wall thickness 10 µm) embedded in the SAXS instrument. The inner volume of the complete system was 11.3 mL.

2.3. Nanoparticle preparation

The nanoparticles were synthesized using the method by Bee [12], which was adapted to the micromixer synthesis. Briefly, an aqueous solution of ferric and ferrous sulfate with a molar ratio of 2:1 Fe(III) to Fe(II) and a total iron concentration of 8.6×10^{-3} mol L^{-1} was prepared. Carboxydextran was added in a weight ratio of 3:1 with respect to the iron salts and then the solution was sparged with nitrogen for 30 minutes. This solution was mixed continuously inside the microreactor with a degassed solution of 25% ammonium hydroxide. The volume ratio of the stream of the iron salts solution to the stream of the ammonium hydroxide solution was 19:1. The experiment was conducted at two different temperatures of 30 °C and 80 °C and three different flow rates of 8 mL min^{-1}, 4 mL min^{-1} and 2 mL min^{-1}. These flow rates represent reaction times of 84 s, 162 s and 326 s before SAXS measurements.

2.4. SAXS measurement

The experiment was performed at the BAM*line* at BESSY (Berlin, Germany) on a Kratky type camera SAXSess (Anton Paar, Austria). The exposure time was 30 s. The measured intensity was corrected by subtracting the intensity of a capillary filled with pure reagent solution. After background correction the data were de-convoluted (slit-length de-smearing). All data processing was performed with the SAXSquant 3.5 software (Anton Paar, Austria). The scattering vector is defined as $q = 4\pi/\lambda \sin(\theta/2)$ with the scattering angle θ and the wavelength $\lambda = 0.154$ nm. The SAXS data evaluation was performed using the Guinier–Porod model [13], where the scattering intensity $I(q)$ is defined by a Guinier contribution at low and a Porod contribution at high q-values:

$$I(q) = \frac{G}{q^s} \exp\left(\frac{-q^2 R_g^2}{3-s}\right) \text{for } q \le q_1 \text{ and}$$

$$I(q) = \frac{D}{q^d} \text{for } q \ge q_1$$

where R_g is the radius of gyration, s is the Guinier exponent, d is the Porod exponent, and G and D are Guinier and Porod scaling factors, respectively. The q-value of transition point q_1 is given by

$$q_1 = \frac{1}{R_g}\left(\frac{(d-s)(3-s)}{2}\right)^{\frac{1}{2}}$$

For data interpretation we used the IRENA program package [14] applied to the model above.

2.5. XRD measurement

The XRD measurement was performed at the µ-Spot beamline at BESSY II Berlin, Germany. The samples were dried on Kapton thin film and measured in transmission with a 100 µm wide beam at an energy of 15 keV. The crystallite size D_{311} was determined from the (311) reflection using a modified Debye–Scherrer- equation

$$D_{311} = \frac{2\pi I(q_{max})}{\int I(q)dq},$$

where $I(q_{max})$ is the scattering intensity at the peak maximum and the denominator is the integral peak width of the (331) reflection.

2.6. XANES measurement

X-ray absorption near-edge structure measurements were carried out at the BAM*line* beamline at BESSY II Berlin, Germany. The dried precipitates were measured in fluorescence mode with standard 45° geometry [15] at the K-edge of iron ($E_o = 7112$ eV). The incident beam intensity was monitored using a 50 mm ionization chamber filled with air at ambient pressure. The energy was scanned using a Si(111) double crystal monochromator with a relative energy resolution of 2×10^{-4}. The XANES scans were carried out in the range from 7032 eV (80 eV below the edge) to 7182 eV (70 eV above the edge) with a step of 1 eV. The fluorescence signal of the characteristic radiation of iron was recorded using a silicon drift detector. The obtained XANES spectra underwent the standard data treatment procedure using Ifeffit 1.2.11c [16].

3. Results and discussion

3.1. SAXS Results

SAXS scattering curves of iron oxide nanoparticles were measured online at different times after mixing of the reagent solutions in the micromixer (see Fig. 1). Nanoparticles could be characterized with sizes in the range of $\pi/q_{max} = 1$ nm to $\pi/q_{min} = 45$ nm. The figures in the top row of Fig. 2 display curves collected during particles formation at 30 °C; the bottom row are corresponding curves of particle formed at 80 °C. We found that the scattering intensities display a characteristic Power law decay of $q^{-1.87}$, $q^{-1.67}$ and $q^{-1.87}$ for reaction times of 84 s, 162 s and 326 s in the q-range between 0.07 nm^{-1} and 0.9 nm^{-1} (Fig. 2 a–c). We assume that these characteristic slopes result from mass fractal structures produced by aggregation of small primary particles.

The scattering intensity in the Porod region scales with $q^{-3.76}$, which is observed for reaction times of 84 s and 162 s at q-values larger than 0.9 nm^{-1}. This scaling is indicative for a rough surface of the primary particles since a q^{-4}- scaling must be expected for particles with a smooth surface. The radius of the primary particles was (1.1 ± 0.1) nm for a reaction time up to 162 s after

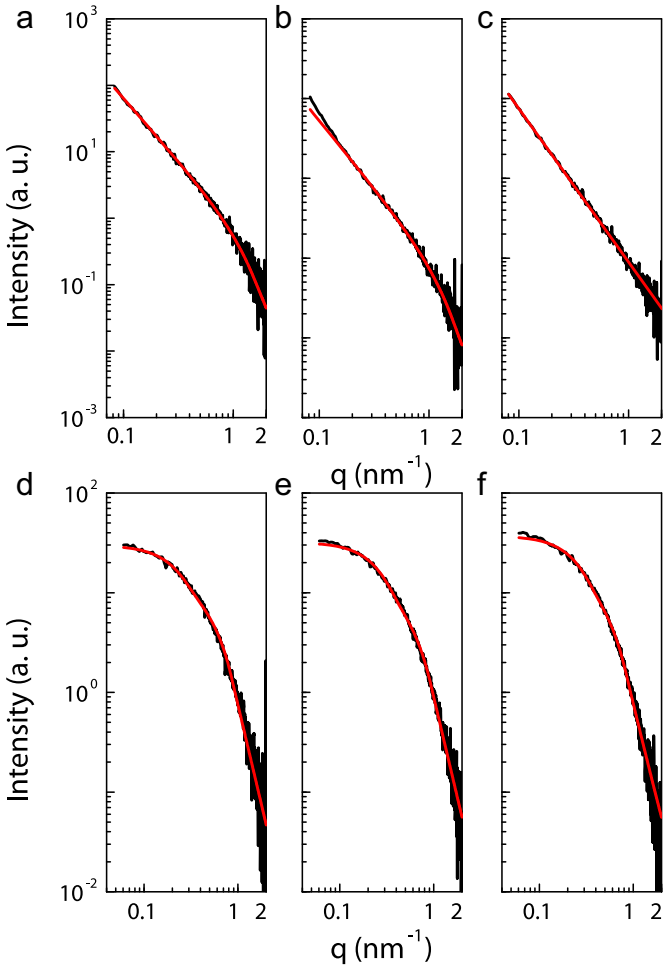

Fig. 2. SAXS curves of iron oxide nanoparticles during the growth process at 30 °C (a–c) and 80 °C (d-e). The time series covers 84 s (a, d), 162 s (b, e) and 326 s (c and f). The solid red lines represent Guinier–Porod fits. The data from the particles synthesized at lower temperature show a distinct slope in the Guinier region which indicates the presence of mass-fractal aggregates.

initialization of the reaction (Note that the uncertainties are the standard deviations of the curve fits using our SASfit program, which was used in metrology studies) [17]. Later, the primary particle radii could not be determined precisely since no Porod-region is found (Fig. 2c). Tentatively, we interpret this as resultant form the coalescence of primary particles to larger aggregates, accompanied by fusion of particle surfaces.

The SAXS data from iron oxide particles formed at an elevated temperature of 80 °C show completely different results. Here, the Guinier-region, visible between 0.07 nm^{-1} and 0.3 nm^{-1}, indicates spherical particles without any signs of aggregation. The

Table 1
Parameters from Guinier–Porod fits: Radii of gyration (R_g), corresponding radii of an equivalent homogenous sphere (R), characteristic exponents (s, d).

Temperature	Time	Guinier		Porod
[°C]	[s]	R_g [nm]; (R [nm])	s	d
30	84	0.8 ± 0.15; (1.1 ± 0.19)	-1.87 ± 0.09	-3.76 ± 0.17
30	162	0.8 ± 0.1; (1.1 ± 0.13)	-1.68 ± 0.06	-3.72 ± 0.12
30	326	< 0.75	-1.87 ± 0.08	–[a]
80	84	2.8 ± 0.2; (3.6 ± 0.25)	0	−4
80	162	2.6 ± 0.2; (3.4 ± 0.25)	0	−4
80	326	3.1 ± 0.2; (4.0 ± 0.25)	0	−4

[a] not available.

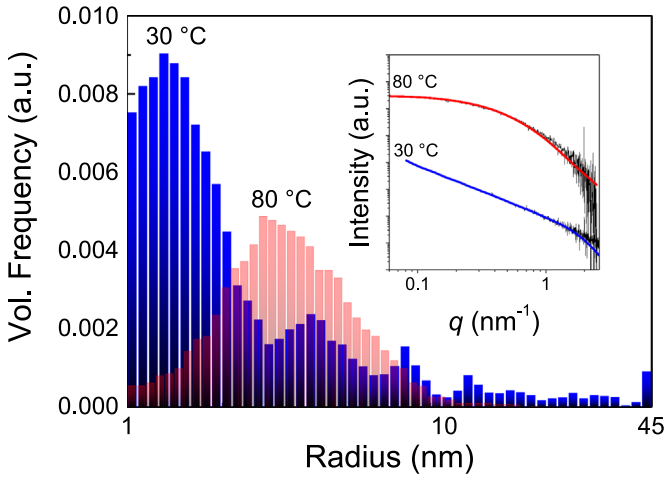

Fig. 3. Volume weighted size distributions of the iron oxide nanoparticles prepared at 30 °C and 80 °C. The inset shows the corresponding SAXS data and curve fits using a Monte Carlo approach [18].

intensities scale with q^{-4} in the Porod region for $q > 0.3$ nm^{-1} as must be expected for a smooth surface. The particle radii were (3.6 ± 0.25) nm at 84 s, (3.4 ± 0.25) nm at 162 s and (4.0 ± 0.25) nm at 326 s. All results are summarized in Table 1.

In addition to the Guinier–Porod model, we applied a Monte-Carlo SAXS data evaluation procedure recently published by Pauw et. al. [18] for determination of the particle size distributions. The result is shown in Fig. 3. From the volume weighted size distributions one can clearly see that the particles prepared at 30 °C display a maximum for diameters slightly larger than 2 nm, which can be attributed to the primary particles. It is also evident that particles up to 45 nm are present, i.e. the particle population is multimodal as expected for multicore particles. In contrast, the size distribution of the particles prepared at 80 °C is monomodal with a mean diameter around 7 nm as it is generally expected for single-core nanoparticles.

It is obvious that the temperature has a strong influence on the particle formation: smaller but unstable particles are formed at 30 °C and stable larger particles at 80 °C. We assume that the reason for this difference is a temperature triggered nucleation and growth process. Based on a cryo-TEM study, Baumgartner et al. [19] proposed a nucleation and growth mechanism of iron oxide nanoparticles. They suggest that the formation process begins with the formation of primary particles from an amorphous phase. These primary particles build branched aggregates. The following particle growth process is dominated by aggregation and coalescence instead of accretion of atoms. Our data support the mechanism proposed by them. The step determining the growth rate of the particles is the absorption of Fe^{2+} by the amorphous ferrous hydroxide phase [20]. This absorption is faster at elevated temperatures. Combined with a higher super saturation and a larger critical nuclei size at higher temperature this may lead to the conclusion that the crystalline phase is formed at 80 °C directly without aggregation and coalescence [21].

TEM measurements were performed to check the SAXS results. Results are shown in Fig. 4. It can be seen that the particles synthesized at 30 °C consist of very small primary particles forming diffuse agglomerates with total diameters of roughly 30 nm. In contrast, the particles synthesized at 80 °C are spherical and well dispersed with diameters of about 7 nm. Therefore, we conclude that the TEM micrographs confirm our findings from SAXS.

Next, we performed XRD measurements to reveal the iron oxide phase and the crystallite size. The nanoparticle suspensions were dried before XRD measurements to gain sufficient intensity.

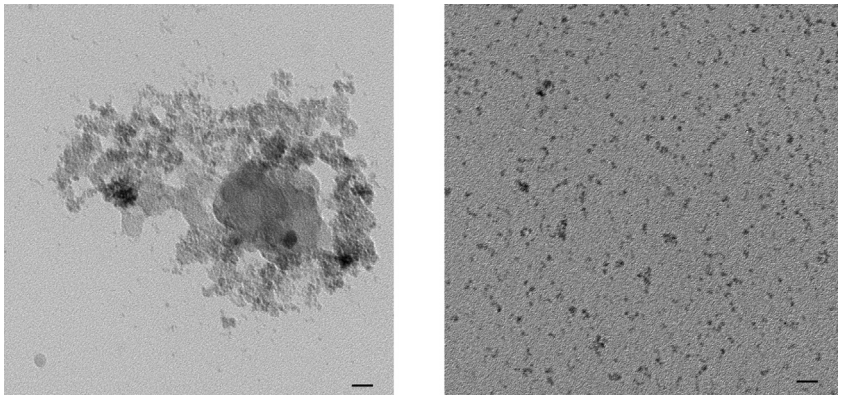

Fig. 4. TEM micrographs from carboxydextran coated iron oxide nanoparticles synthesized at 30 °C (left) and 80 °C (right). Scale bar sizes are 20 nm.

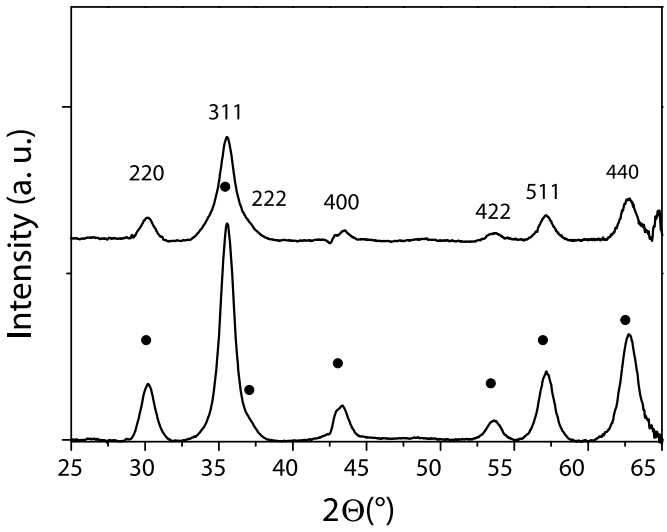

Fig. 5. XRD diffractograms of iron oxide nanoparticles synthesized at 30 °C (top) and 80 °C (bottom). The black dots represent the reflections from γ-Fe_2O_3. Note that Fe_3O_4 exhibits the same set of reflections.

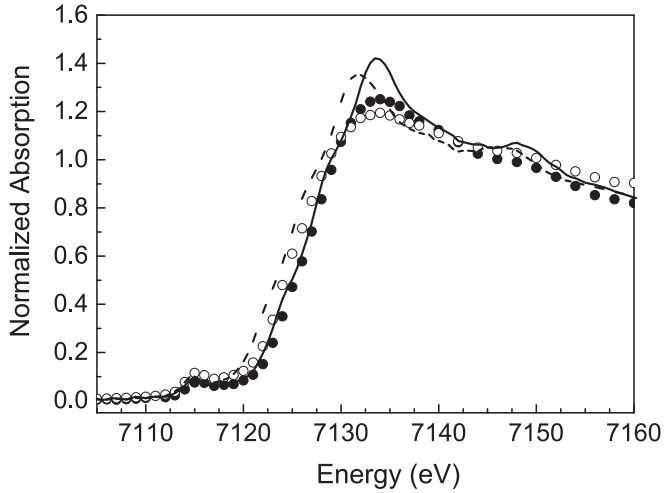

Fig. 6. XANES spectra of iron oxide nanoparticles synthesized at 30 °C and 80 °C (open and filled circles, respectively). Maghemite (dashed line) and magnetite (solid line) are given for comparison.

Fig. 5 shows that the reflex pattern of both particle types can be indexed with the crystal structure of maghemite. The 331 reflection is the most intense and was used to determine the crystallite size by applying the Debye–Scherrer equation. We found a minimum diameter of the crystallites of 6.80 nm for the particles synthesized at 80 °C and 5.53 nm for particles synthesized at 30 °C. These findings are in good agreement with the SAXS results. Since magnetite and maghemite both crystallize in a spinel-type lattice it is not possible to distinguish between these two oxides via X-ray diffraction. Therefore, XANES was employed to determine the iron oxide species. The measured spectra are shown in Fig. 6.

XANES probes the unoccupied electronic states above the Fermi level and is therefore sensitive to the formal valence and the coordination chemistry of the absorbing element. Hence, it can be used as a fingerprint method by comparing the spectra of samples under study with those of neat compounds. In this approach the formal valence can be interpreted as the energy shift of the absorption edge step at half height with respect to the reference spectra. Firstly, the XANES spectra of the iron oxide nanoparticles exhibit a decrease of the intensity of the principal maximum above the absorption edge step (white line) with decreasing particle size, which is typical for nanoparticles in this range of sizes and is associated with the increasing surface-to-volume ratio [22]. The 7 nm particles synthesized at 80 °C have the absorption edge step exactly at the position of that of maghemite (Fig. 6). The same is true for the position of the white-line peak. Thus, the iron oxide species of the 7 nm particles can unambiguously be identified as γ-Fe_2O_3. In the case of the 2 nm particles the absorption edge is at an intermediate position between the absorption edges of magnetite and maghemite indicating that the particle contain besides γ-Fe_2O_3 magnetite, too. This means that in the case of 2 nm particles the oxidation to Fe(III) is not accomplished yet and the nanoparticles contain a significant fraction of Fe(II) ions.

4. Conclusion

Magnetic nanoparticles have successfully been prepared in a micromixer at two different temperatures. Online SAXS analysis revealed two different reaction pathways depending on the synthesis temperature. At lower temperature we assume a mechanism based on the agglomeration and coalescence of amorphous primary particles. At higher temperatures we found no aggregation which leads to the conclusion of direct crystallization. The nanoparticles synthesized at 80 °C were identified as maghemite, whereas the 2 nm particles synthesized at 30 °C most probably consist of a mixed magnetite-maghemite phase.

Acknowledgement

We thank Olga Koshkina for the TEM images, Franziska Emmerling for her help with the XRD measurements, as well as Heinrich Riesemeier and Ralf Britzke for their assistance at the BAMline, Ingo Breßler and Brian R. Pauw for providing the Monte Carlo SAXS evaluation program. Financial support was carried out in the framework of the EU project NanoMag.

References

[1] V. Segal, A. Rabinovich, D. Nattrass, K. Raj, A. Nunes, J. Magn. Magn. Mater. 215 (2000) 513–515.
[2] K. Raj, R. Moskowitz, J. Magn. Magn. Mater. 85 (1990) 233–245.
[3] C.T. Yavuz, J.T. Mayo, W.W. Yu, A. Prakash, J.C. Falkner, S. Yean, L.L. Cong, H. J. Shipley, A. Kan, M. Tomson, D. Natelson, V.L. Colvin, Science 314 (2006) 964–967.
[4] P. Fortina, L.J. Kricka, D.J. Graves, J. Park, T. Hyslop, F. Tam, N.J. Halas, S. Surrey, S.A. Waldman, Trends Biotechnol. 25 (2007) 145–152.
[5] M. Johannsen, U. Gneveckow, L. Eckelt, A. Feussner, N. Waldofner, R. Scholz, S. Deger, P. Wust, S.A. Loening, A. Jordan, Int. J. Hyperth. 21 (2005) 637–647.
[6] D.E. Sosnovik, M. Nahrendorf, R. Weissleder, Circulation 115 (2007) 2076–2086.
[7] A. Jordan, R. Scholz, P. Wust, H. Fahling, J. Krause, W. Wlodarczyk, B. Sander, T. Vogl, R. Felix, Int. J. Hyperth. 13 (1997) 587–605.
[8] D. Kashchiev, Nucleation: Theory and Basic Applications, Butterworth-Heinemann, Oxford, 2000.
[9] W. Ostwald, Z. Phys. Chem. 22 (1897) 289–330.
[10] A. Navrotsky, Proc. Natl. Acad. Sci. USA 101 (2004) 12096–12101.
[11] F. Schonfeld, V. Hessel, C. Hofmann, Lab Chip 4 (2004) 65–69.
[12] A. Bee, R. Massart, S. Neveu, J. Magn. Magn. Mater. 149 (1995) 6–9.
[13] B. Hammouda, J. Appl. Crystallogr. 43 (2010) 716–719.
[14] J. Ilavsky, P.R. Jemian, J. Appl. Crystallogr. 42 (2009) 347–353.
[15] H. Riesemeier, K. Ecker, W. Gorner, B.R. Muller, M. Radtke, M. Krumrey, X-Ray Spectrom. 34 (2005) 160–163.
[16] B. Ravel, M. Newville, J. Synchrotron Radiat. 12 (2005) 537–541.
[17] F. Meli, T. Klein, E. Buhr, C.G. Frase, G. Gleber, M. Krumrey, A. Duta, S. Duta, V. Korpelainen, R. Bellotti, G.B. Picotto, R.D. Boyd, A. Cuenat, Measurement Sci. Technol. 23 (2012) 125005.
[18] B.R. Pauw, J.S. Pedersen, S. Tardif, M. Takata, B.B. Iversen, J. Appl. Crystallogr. 46 (2013) 365–371.
[19] J. Baumgartner, A. Dey, P.H.H. Bomans, C. Le Coadou, P. Fratzl, N. Sommerdijk, D. Faivre, Nat. Mater. 12 (2013) 310–314.
[20] E. Tronc, P. Belleville, J.P. Jolivet, J. Livage, Langmuir 8 (1992) 313–319.
[21] M. Fang, V. Strom, R.T. Olsson, L. Belova, K.V. Rao, Nanotechnology 23 (2012) 145601.
[22] K. Mandel, W. Szczerba, A.F. Thunemann, H. Riesemeier, M. Girod, G. Sextl, J Nanopart Res. 14 (2012) 1066.